Heliyon

ELSEVIER

Received:
26 September 2018
Revised:
23 December 2018
Accepted:
15 February 2019

Cite as: Feng Liu, Dan Han. Petrogenetic and tectonic implications of Triassic granitoids in the Chinese Altay: the Alaer granite example. Heliyon 5 (2019) e01261. doi: 10.1016/j.heliyon.2019.e01261

Petrogenetic and tectonic implications of Triassic granitoids in the Chinese Altay: the Alaer granite example

Feng Liu*, Dan Han

MNR Key Laboratory of Metallogeny and Mineral Assessment, Institute of Mineral Resources, Chinese Academy of Geological Sciences, Beijing, 10037, China

* Corresponding author.

E-mail address: liufeng@cags.ac.cn (F. Liu).

Abstract

Petrogenesis of the Triassic Alaer granite in the Chinese Altay is important to understand the regional crustal evolution. This study found that the biotite granite is metaluminous and high-K calc-alkaline to shoshonitic. The rocks contain low SiO_2 (64.3−68.7 wt.%), high Al_2O_3 (13.46−16.56%) and K_2O (mostly 3.65−7.57 wt.%), and are featured by distinctly higher concentrations of HFSE (e.g., Th, Hf) and ΣREE than those of the nearby Devonian granites. REE patterns show right-inclining trend and weak negative Eu anomalies (δEu = mostly 0.68−0.94), whilst the spidergrams show consistent negative anomalies of Ba, Sr, P, Ti, Nb and Ta and positive anomalies of Th, K, La, Ce, Nd, Zr and Hf. Compared with the local Devonian granites, the Triassic granites have higher calculated initial $^{87}Sr/^{86}Sr$ ratios (0.70601−0.70920) and εNd(t) values −(−1.24 to −0.68). Their Nd model ages (average of 1.08 Ga for one-stage and 1.07 Ga for two-stage) are early Neoproterozoic to late Mesoproterozoic.

We infer that the Triassic Alaer granite belongs to I-type granite and likely formed in an intraplate extensional setting under high temperature (829−885 °C) and pressure (depths of 30−50 km, corresponding to the middle-lower crust in the

https://doi.org/10.1016/j.heliyon.2019.e01261

Chinese Altay region). Granitic magma was produced through the melting of old continental basement with substantial mantle input, triggered by extensional upwelling of mantle-derived magmas. Mixing equation of Nd isotope compositions yielded a 40% of mantle-derived juvenile components for the Alaer granite petrogenesis.

Keywords: Earth sciences, Geochemistry, Geology, Geoscience

1. Introduction

Early Paleozoic to Mesozoic granitic intrusions are widespread in the Central Asian Orogenic Belt (CAOB) (Wang et al., 2010). The Chinese Altay Orogenic Belt is situated in the southwestern CAOB and the south of the Altay Orogenic Belt (AOB). Outcrop of granitoids (including gneissic granites and granitic gneiss) in this belt accounts for about 70% of the whole area (Windley et al., 2002). These granitoids emplaced mainly at the early-middle Ordovician to late Devonian, following some coeval mafic intrusion, and are attributed to be I- or S-type and synorogenic granites in continental arc environment. The oldest intrusion in the region was emplaced at about 460 Ma (Wang et al., 2006; Liu et al., 2008), and the Late Carboniferous to Early Permian intrusions generally occur as stocks and dykes were regarded as I-type, S-type and I-A type in post-collisional extensional setting (Wang et al., 2010).

Large amount of Mesozoic granites (251−180 Ma) develop in the Altay Orogenic Belt (Vladimirov et al., 2005; Annikova et al., 2006; Han, 2008), except for the Chinese Altay. Mesozoic granitoids are relatively rare in the Chinese Altay, and at present only several plutons were identified, such as Jiangjunshan granitic stock (150 Ma, Chen and Jahn, 2002), Shangkelan granitic stock (202 Ma, Wang et al., 2010), Alaer granite (210−212 Ma, Liu et al., 2014a) and related pegmatite dykes (208−210 Mg, Liu et al., 2012). However, their petrogenesis and tectonic setting is still not clear. In this paper, we present new geochemical and Sr-Nd isotope data to determine the genesis and tectonic setting of the late Triassic Alaer granite. It is meaningful to understand Triassic granitic magmatism and the tectonic evolution in the Altay.

2. Geological setting

2.1. Regional geology

The CAOB was formed over prolonged and multiphase subduction and accretion during the Paleozoic (Coleman, 1989; Mossakovsky et al., 1993; Wang et al., 2006; Xiao et al., 2010). The Altay Orogenic belt (AOB) is one of the major units of the CAOB (Sengor et al., 1993). It extends for 2000 km across China, Russia,

https://doi.org/10.1016/j.heliyon.2019.e01261

Kazakhstan and Mongolia, among which about 500 km of its length is within China, and is located between the Siberian and Kazakhstan-Junggar plates (Fig. 1a). The Altay Orogenic belt is a collage of continental blocks, island arcs, ophiolites and other accretionary complexes (Sengor et al., 1993; He et al., 1994). For the Chinese Altay, it is divided into a northern part that contains the North Altay (the Devonian-Carboniferous Nurter volcanic-sedimentary basin) and the Central Altay (the Kanas-Keketuohai Paleozoic magmatic arc), and the southern part that contains the South Altay (the Devonian-Carboniferous Kelan back-arc basin, the Carboniferous-Permian Karba-Naleimu magmatic arc, the Carboniferous Xikaerba fore-arc basin) and the Erqis-Buergen tectonic mélange (He et al., 2004; Wang et al., 2010) (Fig. 1a).

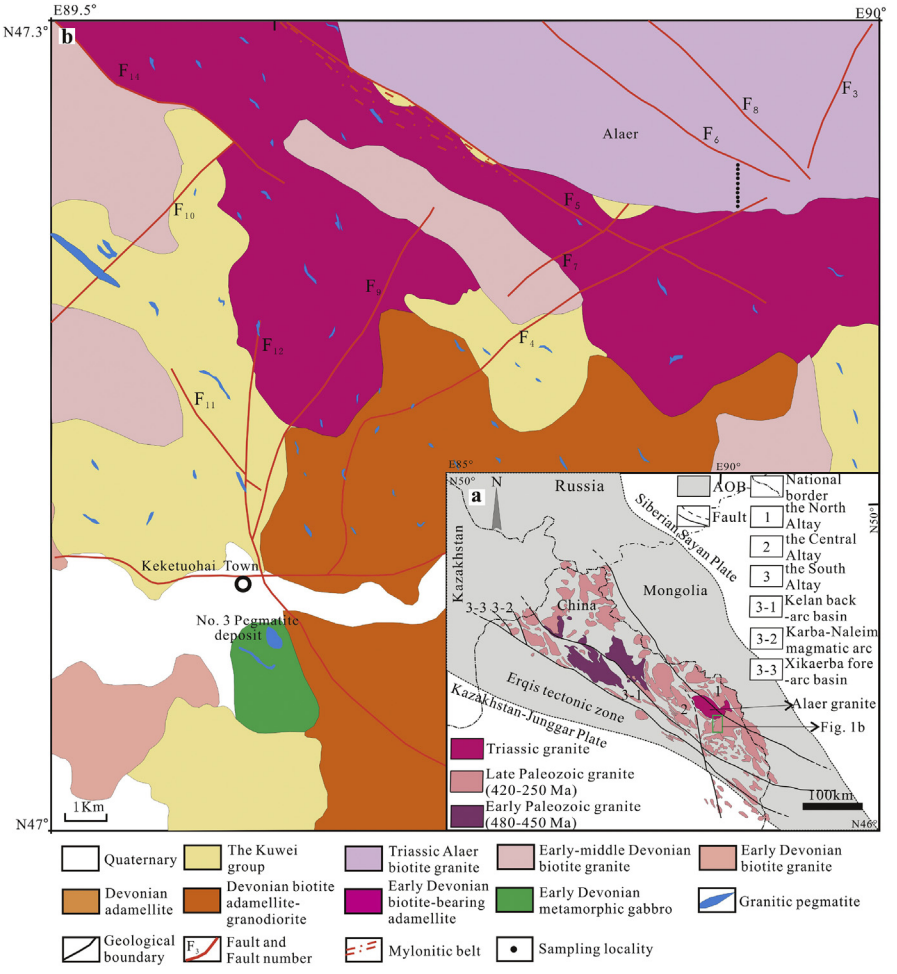

Fig. 1. Simplified maps showing (a) tectonic sketch and distribution of granite in the Chinese Altay. The Alaer granite is only Triassic pluton identified and located within the Paleozoic Kanas-Keketuohai magmatic arc (Modified from He et al., 2004 and Song et al., 2017); (b) The outcrops are mainly Early Devonian plutons, the Paleozoic metasedimentary rocks (Kuwei group) and the northeastern Alaer granite (Modified from Zou and Li, 2006).

https://doi.org/10.1016/j.heliyon.2019.e01261

In terms of tectonic evolution, the Late Neoproterozoic to Early Paleozoic Altay Orogen was likely marked by a stable continental margin setting (He et al., 1990), and bipolar crustal accretion commenced in the Paleozoic: Oceanic plate subduction likely took place in the Ordovician to Devonian, and an active continental margin began to develop in the Late Ordovician (ca. 460 Ma, Wang et al., 2006). The Late Devonian-Early Carboniferous arc-continent collision had established the main tectonic framework of the Altay Orogen (He et al., 1994; Windley et al., 2002; Li et al., 2003), following the Late Carboniferous-Early Permian post-collisional extension (Wang et al., 2010) and the Mesozoic-Cenozoic relatively stable continental development (Li and Poliyangsiji, 2001).

The Kanas-Keketuohai region in the northern-middle Chinese Altay is mainly composed of Early Paleozoic metamorphic rocks, and there are many outcrops of Sinian-Middle Ordovician low-grade metamorphosed thick terrigenous flysch (Habahe Group), Upper Ordovician volcanics/molasse and terrigenous clastic formations (Dongxileke and Baihaba formations), and Middle and Upper Silurian metasandstone (Kulumuti Formation). Granitic rocks, mostly Early Devonian, are widespread in the region. Rock types include gneissic biotite monzogranite, gneissic biotite granite, gneissic tonalite, biotite granite, and two-mica granite (Liu et al., 2009).

The Alaer granite is located within the Paleozoic Kanas-Keketuohai magmatic arc (He et al., 2004). The Sinian-Lower Paleozoic country rocks of the granites are strongly metamorphosed, forming gneiss and schist. The granites are mainly Early Devonian and minor Mesozoic (the latter includes the Alaer and Shangkelan plutons). There are some outcrops of the Early-Devonian metamorphosed basic rocks as well. The bedding of the country rocks, the fold axis and the associated faults in the region are all NW-trending (Zou and Li, 2006; Wang et al., 2010).

2.2. Local geology and petrography

The Alaer granite is situated in the northeastern Keketuohai mining area (Fig. 1b). The pluton extends along the trend of the Altay orogen and intruded into the Paleozoic metasedimentary rocks (Kuwei group) and Devonian plutons. The outcrops of the Alaer granite have experienced strong spherical weathering (Fig. 2a). The

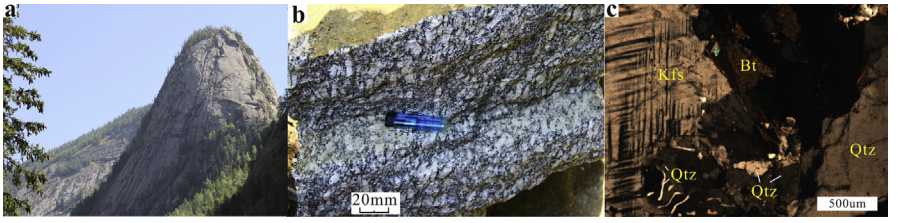

Fig. 2. Field and microscopic photographs of the Alaer granite showing (a) strong spherical weathering, (b) gray coarse-grained porphyritic biotite granite, (c) microcline as lattice twin and micrographic texture under crossed polars.

https://doi.org/10.1016/j.heliyon.2019.e01261

northern part of the pluton is cut through by a regional fault (Fig. 1a), whereas the southern, eastern and western boundaries of the pluton are marked by rare metals-hosting pegmatite veins. There are over 2100 pegmatite veins around the granite. Away from the contact, these veins change from simple to composite in composition and the rare metal mineralization intensity increases. The study of Zou and Li (2006) proposed that the pegmatite veins and the rare metal mineralization are closely related to the Alaer granite.

Our field studies suggest that the Alaer granite contains gray coarse-grained porphyritic biotite granite. The phenocrysts (30−60%) comprise mainly microcline (5 × 15 mm in size; up to 2 × 5 cm) (Fig. 2b). The porphyritic biotite granite is gneissic with biotite lineation. It comprises mainly phenocrysts of K-feldspar (45−50% of total phenocrysts, the same below), plagioclase (5−10%), quartz (20−25%), biotite (10−15%). The groundmass is composed of microcline (20% of total rock, the same below), An (10−30) plagioclase (10%), quartz (20%) and biotite (5%) (Fig. 2c). Accessory minerals include mainly magnetite, ilmenite, zircon, apatite, sphene and minor monazite. Most K-feldspars are xenomorphic, and some K-feldspar grain margins are filled with vermicular quartz, showing micrographic texture resulted from eutectic crystallization. Plagioclase is hypidiomorphic and columnar, locally vermicular in shape.

3. Methods

3.1. Sampling

The samples were collected in the southern part of the Alaer pluton along a new roadcut. Sampling was taken in a 1 km spacing (Fig. 1b), and over 0.5 kg fresh sample was collected in each site. Major and trace element analyses of ten samples and Sr-Nd isotopic analyses of six samples were conducted.

3.2. Analytical methods

Whole-rock analyses were done in the National Research Center for Geoanalysis, Chinese Academy of Geological Sciences (CAGS, Beijing). Rb, Sr, Sm and Nd isotopes were analyzed at the Isotope Laboratory of Institute of Geology, CAGS. For major element compositions, X-ray fluorescence spectrometer (PW4400) was used, using the Chinese national standard GBW07103 and GBW07104 for the calibrations of FeO and the rest major element compositions, respectively. The analytical errors are generally less than 2%. For trace element compositions, ICP-MASS (X-series) and ICP-AES (IRIS) were used, using standards of JY/T015-1996 and DZ/T0223-2001 for calibration, respectively. Precision is estimated to be 5% and accuracy is better than 5%. The isotope dilution method was used for the analysis of Rb, Sr, Sm and Nd. Their concentrations and Sr isotopic compositions were

https://doi.org/10.1016/j.heliyon.2019.e01261

measured by a Finnigan MAT262 multi-collector (MC) thermal ionization mass spectrometer (TIMS), using $^{88}Sr/^{86}Sr = 8.37521$ as calibration of isotopic mass-dependent fractionation. Nd-isotope compositions were measured by a Nu Plasma high-resolution (HR) MC-ICP-MS and DSN-100, using $^{146}Nd/^{144}Nd = 0.7219$ as calibration.

4. Results

Whole-rock geochemical data of the Alaer granite are given in Table 1. The Alaer biotite granite has lower and narrow range of SiO_2 contents (64.3−68.7 wt.%) than the Paleozoic granites (>70 wt.%) in the region, and moderate Al_2O_3 contents (13.46−16.56 wt.%). In general, the granites are K_2O-rich (mostly 3.65−7.57 wt.%) with ($K_2O + Na_2O$) of 6.24−10.43 wt.%. The CaO, ($Fe_2O_3 + FeO$), MgO, TiO_2 and P_2O_5 contents are of 1.73−3.01 wt.%, 2.81−5.26 wt.%, 0.85−1.61 wt.%, 0.56−1.14 wt.% and 0.30−0.57 wt.%, respectively. K_2O/Na_2O ratios range from 0.73 to 2.65 (only KKTH-5 below 1). Large variation of Rittmann index σ (1.5−4.9) indicates alkaline (3.3−4.9 for KKTH-4, 9, 10) and calc-alkaline (<3.3 for the other seven samples) affinities. In the K_2O vs. SiO_2 diagram (Fig. 3a), the data points mostly scatter in the high-K calc-alkaline to shoshonitic fields with the exception of KKTH-5. The samples have similar A/CNK (0.97−1.03) close to 1, and are thus mainly metaluminous (Fig. 3b).

The HFSE concentrations of the Triassic Alaer granite are mostly higher than those of the Devonian granites in the Keketuohai area (Liu et al., 2014b). The LILE concentrations are higher than the average crust, with the Rb/Sr ratios below 1. The total REE (ΣREE) concentrations of 124.6−627.8 ppm are distinctly higher than those of the Devonian granites in the region. Chondrite-normalized REE patterns (Fig. 4a) show distinctly LREE enrichment (LREE/HREE = 7.27−21.07, $(La/Yb)_N$ = 8.39−38.97, $(La/Sm)_N$ = 1.84−4.59 and $(Gd/Yb)_N$ = 1.48−3.36) (Table 1) and mostly weak negative Eu anomalies (δEu = 0.68−0.94) with the exception of sample KKTH-4 (δEu = 1.37) (Table 1; Fig. 4a). In the primitive mantle-normalized multi-element spidergrams (Fig. 4b), all samples show consistent patterns with negative anomalies in Ba, Sr, P, Ti, Nb and Ta, and positive anomalies of Th, K, La, Ce, Nd, Zr and Hf.

The Sr-Nd isotopic analytical results for the Alaer granite are given in Table 2. Initial Sr-Nd isotope compositions and εNd(t) values have been calculated at 211.4 Ma (zircon U-Pb age of the Alaer granite, Liu et al., 2014a). Compared with the Devonian granites in the region (Liu et al., 2014b), the Alaer granite has relatively low ratios and narrow range of $^{87}Rb/^{86}Sr$ (0.877−1.794), $^{87}Sr/^{86}Sr$ (0.709837−0.712471), $^{147}Sm/^{144}Nd$ (0.0959−0.1381) and Rb/Sr (<1), implying that the initial Sr-isotopic compositions are meaningful (Romer et al., 2012). The

https://doi.org/10.1016/j.heliyon.2019.e01261

Table 1. Major (wt%) and trace (ppm) elements data for the Alaer granite.

	Number	KKTH-1	KKTH-2	KKTH-3	KKTH-4	KKTH-5	KKTH-6	KKTH-7	KKTH-8	KKTH-9	KKTH-10	GBW07103		detection limit (ppm)
												Recommended values	This study	
	SiO_2	64.27	65.73	65.73	65.18	68.29	68.74	65.46	66.15	68.30	66.53	72.83	72.84	
	Al_2O_3	14.93	14.63	15.00	16.56	14.07	13.46	14.78	14.98	14.87	15.32	13.40	13.38	
	CaO	2.91	3.01	2.83	1.73	2.75	2.41	2.63	2.67	1.73	2.07	1.55	1.58	
	Fe_2O_3	2.21	1.75	1.64	1.24	1.39	1.65	2.03	1.74	1.05	1.45	0.94	0.90	
	FeO	3.05	3.04	2.64	1.78	2.60	2.46	2.69	2.30	1.76	2.30			
	K_2O	4.07	3.65	4.23	7.57	2.64	4.20	4.60	4.86	6.31	5.65	5.01	4.90	
	Na_2O	3.30	3.42	3.40	2.86	3.60	2.99	3.20	3.23	2.76	3.12	3.13	2.90	
	MgO	1.61	1.45	1.32	0.85	1.30	1.13	1.45	1.22	0.86	1.10	0.42	0.37	
	MnO	0.09	0.09	0.08	0.05	0.08	0.07	0.08	0.07	0.05	0.07	0.06	0.06	
	P_2O_5	0.57	0.56	0.45	0.32	0.47	0.41	0.52	0.45	0.30	0.40	0.098	0.09	
	TiO_2	1.14	1.09	0.95	0.58	0.87	0.81	1.00	0.84	0.56	0.73	0.28	0.29	
	CO_2	0.43	0.26	0.60	0.43	0.43	0.26	0.26	0.34	0.34	0.26			
	H_2O^+	0.70	0.40	0.42	0.38	0.56	0.40	0.44	0.40	0.30	0.42			
	LOI	0.50	0.42	0.60	0.45	0.44	0.35	0.37	0.55	0.31	0.45			
	total	99.28	99.08	99.89	99.98	99.49	99.34	99.51	99.80	99.50	99.87			
	$Na_2O + K_2O$	7.37	7.07	7.63	10.43	6.24	7.19	7.80	8.09	9.07	8.77			
Ratio	A/NK	1.52	1.53	1.47	1.28	1.60	1.42	1.44	1.41	1.31	1.36			
	A/CNK	0.99	0.97	0.98	1.03	1.02	0.97	0.98	0.97	1.02	1.02			
	DI	74.9	75.4	77.2	84.9	77.2	80.2	77.6	79.0	85.1	81.8			
	$Mg^{\#}$	0.37	0.36	0.37	0.35	0.38	0.34	0.37	0.36	0.36	0.35			
	Rb	213	202	206	298	211	196	224	206	265	269	466	469	1.0

(*continued on next page*)

https://doi.org/10.1016/j.heliyon.2019.e01261

Table 1. (*Continued*)

Number	KKTH-1	KKTH-2	KKTH-3	KKTH-4	KKTH-5	KKTH-6	KKTH-7	KKTH-8	KKTH-9	KKTH-10	GBW07103		detection limit (ppm)
											Recommended values	This study	
Ba	841	740	885	1384	345	624	885	945	1154	870	343	329	0.5
Th	15.7	19.8	46.0	28.8	33.9	39.3	10.5	23.0	63.2	59.0	54	50.1	0.8
U	3.72	3.50	3.17	2.27	2.70	2.22	2.18	2.51	2.35	3.17	18.8	19.3	0.003
Ta	2.67	3.65	1.94	1.28	2.06	1.45	1.47	2.06	1.72	2.06	7.2	7.1	0.05
Nb	35.4	38.2	35.3	31.4	35.1	24.5	27.2	26.9	30.5	26.5	40	40	0.01
Sr	392	396	389	378	294	311	392	396	323	325	106	92.2	0.2
Zr	556	506	379	344	438	389	457	432	280	431	167	152	0.05
Hf	15.3	14.0	10.2	9.6	12.8	11.1	11.9	11.7	8.0	12.3	6.3	5.72	0.01
Li	62.7	58.4	55.7	54.1	88.2	56.9	61.2	51.0	52.5	69.7	131	141	1.0
B	<2	<2	<2	<2	<2	<2	<2	<2	3.02	<2			2.0
Sc	13.6	12.8	12.0	7.7	11.4	10.5	12.6	10.7	7.4	9.5	6.1	6.14	0.1
V	86.3	76.4	66.5	44.2	60.1	62.3	74.1	62.5	40.7	56.9	24	22.6	2.0
Cr	11.4	9.7	6.1	9.6	9.1	12.0	13.8	6.8	7.2	18.4	3.6	2.02	1.0
Co	9.12	8.49	7.33	5.21	8.02	7.92	5.47	9.02	4.97	6.87	3.4	2.93	0.2
Ni	9.16	8.75	6.21	6.09	8.30	7.61	8.76	5.92	4.89	9.49	2.3	1.06	1.0
Cu	35.7	29.0	25.6	19.9	24.0	22.5	24.5	24.6	16.8	25.0	3.2	2.72	0.2
Pb	24.3	23.4	27.5	43.7	21.2	24.4	26.6	29.0	39.9	36.5	31	32.8	0.1
Zn	128.0	117.0	102.0	67.7	113.0	91.4	116.0	94.3	66.8	88.3	28	29.1	2.0
Ga	25.2	25.5	25.4	22.5	25.9	22.4	24.6	23.8	22.1	24.2	19	19.3	0.2
Ge	1.42	1.46	1.58	1.27	1.42	1.38	1.34	1.43	1.52	1.53			0.01
As	1.09	1.18	1.38	0.61	0.89	1.05	0.85	1.07	1.45	1.27			1.0
Mo	0.50	0.45	0.23	0.13	0.11	0.15	0.25	0.32	0.06	0.06	3.5	3.49	0.05
Se	0.02	0.03	0.02	0.02	0.03	0.02	0.01	0.02	0.04	0.02			0.01
La	62.0	72.1	129.0	24.9	69.4	84.1	42.4	83.3	138.0	88.4	54	52.5	0.01
Ce	130.0	149.0	266.0	37.1	125.0	164.0	94.3	163.0	273.0	170.0	108	104	0.01
Pr	19.1	21.7	34.4	6.8	17.7	21.1	12.7	22.0	34.4	21.4	12.7	12.3	0.01

https://doi.org/10.1016/j.heliyon.2019.e01261

Table 1. (*Continued*)

	Number	KKTH-1	KKTH-2	KKTH-3	KKTH-4	KKTH-5	KKTH-6	KKTH-7	KKTH-8	KKTH-9	KKTH-10	GBW07103		detection limit (ppm)
												Recommended values	This study	
	Nd	83.7	92.9	133.0	29.0	69.7	82.2	53.0	91.4	131.0	84.4	47	45.1	0.01
	Sm	16.60	18.40	21.70	8.72	12.10	13.30	11.60	16.50	19.40	14.50	9.7	9.43	0.01
	Eu	3.52	3.70	4.12	3.05	2.44	2.68	2.98	3.56	3.56	3.03	0.85	0.8	0.003
	Gd	11.10	12.70	12.30	4.11	9.03	8.92	6.95	7.26	9.87	10.80	9.3	8.07	0.01
	Tb	2.04	2.42	2.19	0.85	1.49	1.51	1.43	1.87	1.56	1.52	1.65	1.59	0.003
	Dy	11.10	13.60	12.20	4.43	8.19	8.00	7.32	10.40	9.07	7.77	10.2	9.73	0.003
	Ho	1.71	2.13	1.53	0.73	1.20	1.05	1.16	1.52	0.93	0.97	2.05	2	0.003
	Er	5.42	6.86	5.16	2.23	4.06	3.68	3.74	4.96	3.83	3.64	6.5	6.18	0.003
	Tm	0.62	0.79	0.40	0.27	0.47	0.39	0.45	0.53	0.29	0.33	1.06	1.05	0.003
	Yb	4.64	5.66	3.03	2.13	3.59	2.89	3.35	4.05	2.54	2.85	7.4	7.4	0.01
	Lu	0.70	0.82	0.43	0.32	0.53	0.44	0.50	0.59	0.36	0.44	1.15	1.16	0.003
	Y	44.8	55.4	41.0	28.2	32.8	27.8	32.8	40.6	27.7	27.3	62	64.7	0.01
	ΣREE	352.25	402.78	625.46	124.63	324.90	394.26	241.88	410.94	627.81	410.05			
	LREE	314.92	357.80	588.22	109.56	296.34	367.38	216.98	379.76	599.36	381.73			
	HREE	37.33	44.98	37.24	15.07	28.56	26.88	24.90	31.18	28.45	28.32			
Ratio	LREE/HREE	8.44	7.95	15.80	7.27	10.38	13.67	8.71	12.18	21.07	13.48			
	$(La/Yb)_N$	9.58	9.14	30.54	8.39	13.87	20.87	9.08	14.75	38.97	22.25			
	δEu	0.75	0.70	0.70	1.37	0.68	0.71	0.94	0.86	0.70	0.71			
	δCe	0.92	0.91	0.96	0.69	0.85	0.93	0.99	0.91	0.94	0.93			

https://doi.org/10.1016/j.heliyon.2019.e01261

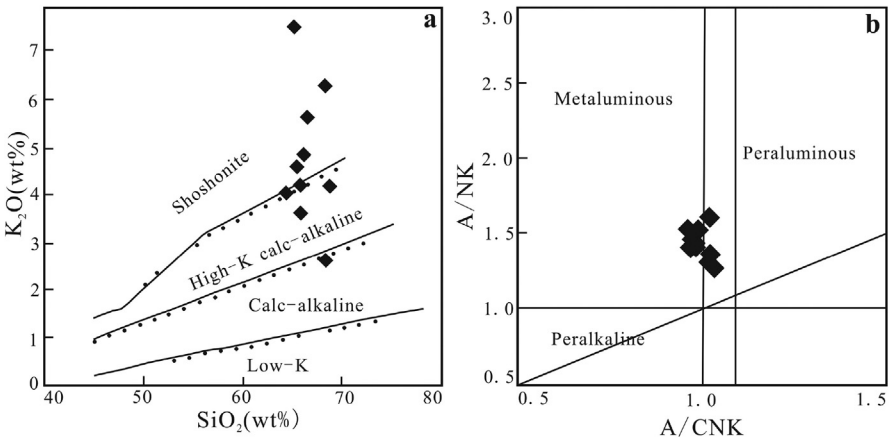

Fig. 3. Classification of the Alaer granite samples: (a) SiO_2 − K_2O diagram (Rickwood, 1989). (b) A/CNK − A/NK diagram (Maniar and Piccoli, 1989). (A/NK = molar ratio of $Al_2O_3/[K_2O + Na_2O]$; A/CNK = molar ratio of $Al_2O_3/[CaO + K_2O + Na_2O]$).

$^{143}Nd/^{144}Nd$ (0.51245−0.51251) and calculated initial $^{87}Sr/^{86}Sr$ (0.70601−0.70920) ratios are high compared to the Devonian granites in area. εNd(t) values range from −1.24 to −0.68, which are higher than those (−3.07 to -2.16) of the Devonian granites in the region (Liu et al., 2014b). Their $f_{Sm/Nd}$ values −(−0.51 to −0.30) fall in a range of −0.6 to −0.2, Sm/Nd ratios range from 0.159 to 0.228, and their average one-stage Nd model ages (t1DM = 1.08 Ga) is very similar to that of two-stage Nd model ages (t2DM = 1.07 Ga), displaying a low-degree fractionation and homogeneous isotopic system (Kovalenko et al., 2004).

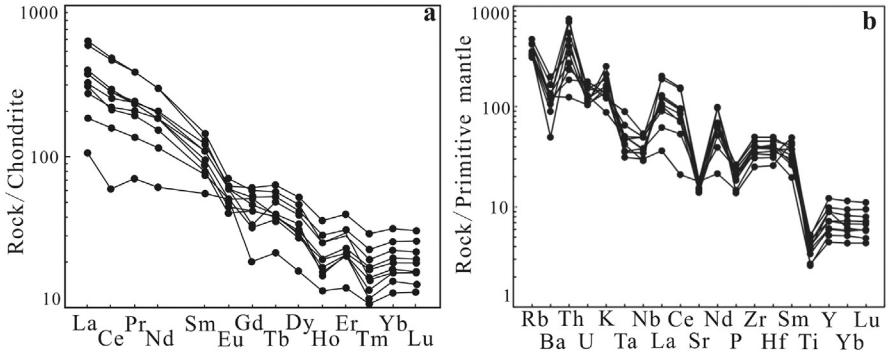

Fig. 4. The chondrite-normalized REE (a) and trace element concentrations normalized to the primitive mantle (b) for the Alaer granite. Primitive mantle and chondrite normalization values are from Sun and McDonough (1989).

https://doi.org/10.1016/j.heliyon.2019.e01261

Table 2. Sr-Nd concentrations (ppm) and isotopic composition of the Alaer pluton.

Sample	KKTH-1	KKTH-2	KKTH-3	KKTH-4	KKTH-5	KKTH-6
Rb	173.9	156.9	165.3	237.0	70.0	153.4
Sr	385.0	387.0	389.0	382.0	230.9	310.3
$^{87}Rb/^{86}Sr$	1.307	1.173	1.229	1.794	0.877	1.431
$^{87}Sr/^{86}Sr$	0.709943	0.709837	0.710007	0.712471	0.711842	0.711208
$\pm 2\sigma$	0.000013	0.000014	0.000015	0.000014	0.000015	0.000015
$(^{87}Sr/^{86}Sr)_i$	0.70601	0.70631	0.70631	0.70708	0.70920	0.70691
$\varepsilon Sr(t)$	25.1	29.3	29.4	40.3	70.4	37.8
Sm	13.43	14.92	17.74	5.56	8.06	11.00
Nd	64.77	69.43	101.96	24.35	41.74	69.34
$^{147}Sm/^{144}Nd$	0.1254	0.1300	0.1028	0.1381	0.1168	0.0959
$^{143}Nd/^{144}Nd$	0.51250	0.51251	0.51247	0.51251	0.51246	0.51245
$\pm 2\sigma$	0.000006	0.000007	0.000010	0.000007	0.000009	0.000006
$(^{143}Nd/^{144}Nd)_i$	0.512324	0.512331	0.512330	0.512318	0.512303	0.512313
$\varepsilon Nd(t)$	−0.83	−0.68	−0.70	−0.94	−1.24	−1.05
T_{1DM} (Ga)	1.13	1.17	0.93	1.29	1.08	0.91
T_{2DM} (Ga)	1.06	1.05	1.05	1.07	1.09	1.08
$f_{Sm/Nd}$	−0.36	−0.34	−0.48	−0.30	−0.41	−0.51
$f_{Rb/Sr}$	14.80	13.18	13.86	20.69	9.61	16.30

5. Discussion

5.1. Triassic magmatism in the Altay Orogenic Belt

Magmatism and mineralization in the CAOB was long regarded to occur dominantly in Paleozoic. However, recent geochronologic studies show that Mesozoic magmatism was also present in the belt, e.g., the Triassic granitic magmatism in the Xingmeng, East Tianshan, West Tianshan and Altay orogenic belt (Zhou et al., 2000; Yang et al., 2012; Li et al., 2003; Wang et al., 2010). In Xinjiang (NW China), Triassic magmatic-hydrothermal events are suggested to have been closely related to some large-scale ductile shear zones and the related gold-rare metal mineralization (Zhu, 2007).

A large-scale Triassic granitic magmatism develops in the Altay orogenic belt. In the Mongolian, Russian and Kazakhstan Altay, the Triassic magmatism was developed mainly during ca. 245−196 Ma (commonly divided into the 245−228 Ma and 225−196 Ma phase). The older 245−228 Ma magmatic phase had generated biotite and two-mica granodiorite, monzogranite and leucogranite, which are intruded by the aplitic to pegmatitic muscovite-(tourmaline) leucogranite stocks or dykes (Han, 2008). The younger 225-196 Ma phase is mainly developed in the Mongolian

https://doi.org/10.1016/j.heliyon.2019.e01261

Altay (e.g., the leucogranites in the Chigerte and Sagsai terranes (225 ± 10 Ma), Demin et al. (2001)) and the Russian Altay (e.g., the Triassic leucogranites (Vladimirov et al. (2005)) and alkaline mafic dykes (Pavlova et al. (2008))). Rock types include porphyritic granite, tourmaline-bearing granite, porphyritic amphibole-bearing biotite granite, biotite granite, amphibole-bearing biotite syenite, granosyenite, alaskite, ongonite and spodumene-bearing granite (Kozlov et al., 1991). Triassic granites in Chinese Altay were identified only recently by high precision zircon dating, and at present only the Shangkelan and Alaer pluton were confirmed to be Triassic (Wang et al., 2008; Liu et al., 2014a). However, the outcrop of large number of Triassic pegmatite veins implies that Triassic granitic magmatism also develops in the Chinese Altay. Previous study also indicated that Triassic pegmatites and related rare metal (e.g., Mo, W, Li, Ta, Be and Cs) mineralization have close relationship with the coeval granites (Zou and Li, 2006; Zhu et al., 2006; Wang et al., 2008; Liu et al., 2014a).

5.2. Petrogenesis

The Alaer granite doesn't contain early crystallizing peraluminous minerals such as cordierite, muscovite, and garnet (Fig. 2), and the samples have similar A/CNK (0.97−1.03), suggesting that its parental magma was metaluminous. These samples plot within the high-K calc-alkaline and shoshonitic fields in Fig. 3 and have alumina saturation index (A/CNK) less than1.1, suggesting that it belongs to I-type and/or A-type granites, according to the criteria of Chappell and White (1992). In terms of trace element geochemistry, all the Alaer granite samples show high Zr, Hf, Ga concentrations and Ga/Al ratios (2.53−3.14, with an average of 2.8), as well as positive anomalies in Th, K, La, Ce, Zr and Hf, and negative anomalies in Ti, P, Sr and Ba in the spidergram (Fig. 4b), sharing A-type features somewhat (Collins et al., 1982; Whalen et al., 1987). However, their low SiO_2, absence of significant Eu negative anomaly in REE pattern and depleted Nb, Ta in the spidergram are completely inconsistent with typical A-type granite and more in line with some kind of I-type granite. This granite displays the negative correlation between P_2O_5 and SiO_2 (Fig. 5a) and the positive correlation between A/CNK and SiO_2 (Fig. 5b), consistent with the common features of I-type granites (Chappell, 1999; Clemens et al., 2011; Clemens and Stevens, 2012), thus suggesting it is I-type granite.

Physio-chemical conditions can significantly affect granite composition. Zircon is an early-crystallizing accessory mineral in granitic magmas that is very sensitive to temperature (Miller et al., 2003), thus its saturation temperature (T_{Zr}) can be regarded to approximate the near-liquidus temperature of granitic rocks (King et al., 1997). Granitic magma temperatures are typically estimated using the zircon saturation thermometer according to Watson and Harrison (1983). The Alaer granite samples yield the calculated T_{Zr} values of 829 °C−885 °C (Table 3) which represent

https://doi.org/10.1016/j.heliyon.2019.e01261

(1989)

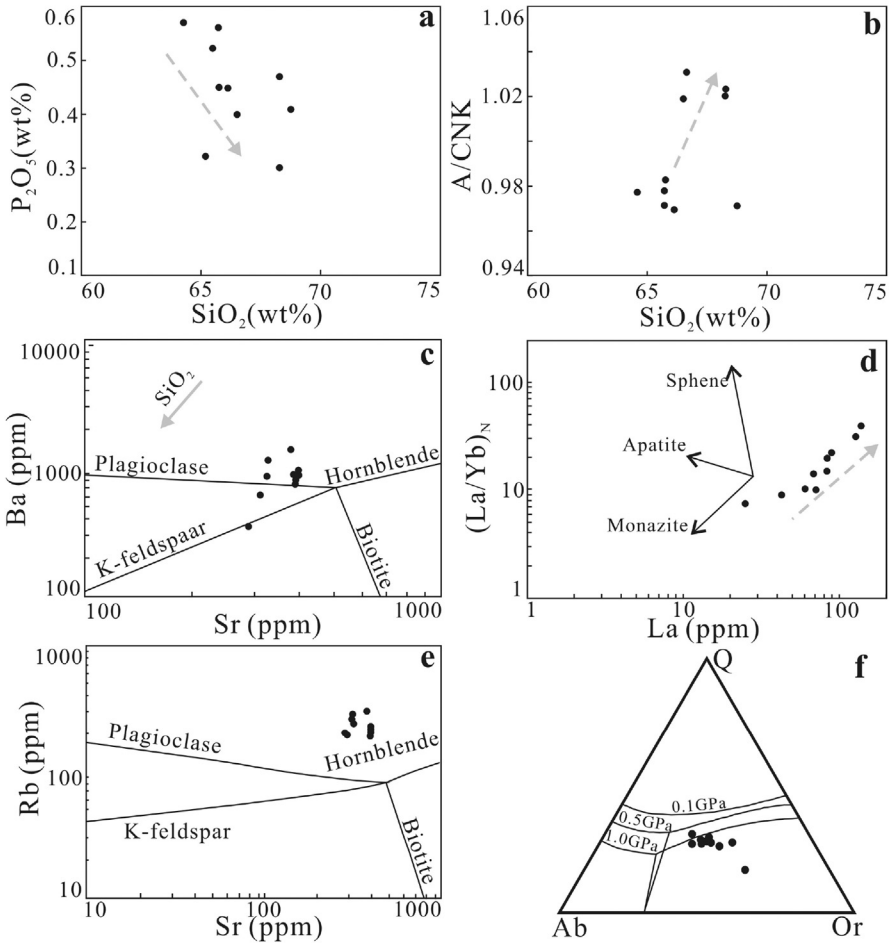

Fig. 5. Plots of (a) P_2O_5 vs. SiO_2, (b) A/CNK vs. SiO_2, (c) Ba vs. Sr, (d) $(La/Nb)_N$ vs. La, and (e) Rb vs. Sr for the Alaer granite, illustrating that mineral fractionation is responsible for chemical compositions of the granite. Mineral fractionation vectors from Nash and Crecraft (1985), Bacon and Druitt (1988), Mahood and Hildreth (1983), Arth (1976). The average crustal composition from Weaver and Tarney (1984) is assumed to represent the initial melt composition. Grey dotted lines with arrows in (a), (b) and (d) show evolution trend of trace element concentrations. Plot of (f) CIPW-normative Q-Ab-Or diagram (Johannes and Holtz, 1996), showing the melt composition of the Alaer granite under high pressure. Q-quartz, Ab-albite, Or-orthosite.

minimum estimates of the true magmatic temperature because of the observed negative correlation between Zr and SiO_2 and the lack of inherited zircon grains. It suggests a hot granitic magma with little residue, whose formation involved external heat input (Miller et al., 2003).

The weak depletions in Sr, Ba, and Eu slightly negative-positive anomaly of the Alaer granite suggests that it might originate from source with less fractionation or residue of plagioclase in melting. Compared with the Devonian granites in the

https://doi.org/10.1016/j.heliyon.2019.e01261

Table 3. The results of estimated zircon saturation temperatures.

Number	KKTH-1	KKTH-2	KKTH-3	KKTH-4	KKTH-5	KKTH-6	KKTH-7	KKTH-8	KKTH-9	KKTH-10
M	1.64	1.64	1.63	1.58	1.49	1.56	1.62	1.63	1.50	1.55
whole rock Zr (ppm)	556	506	379	344	438	389	457	432	280	431
lnDZr	6.79	6.89	7.18	7.27	7.03	7.15	6.99	7.05	7.48	7.05
T_{Zr} (°C)	885	875	848	843	874	856	866	860	829	867

https://doi.org/10.1016/j.heliyon.2019.e01261

region, the pluton shares lower SiO_2 and differentiation index (DI, < 80) and obviously higher P_2O_5, Fe_2O_{3T}, MgO and TiO_2 concentrations. The evolution of trace elements also shows that La and $(La/Yb)_N$, Ba and Sr, Rb and Sr are positively correlated (Fig. 5c, d, e). These all reflected the less fractionation of feldspar, apatite, monazite, and Fe-Ti oxides from the magma. In summary, during formation of the granite, magma likely underwent a low-degree fractionation process.

Granitic magma with little plagioclase residue in melting means high pressure setting (>30 km) in magma source. The Alaer granite with LREE enrichment, strong HREE depletion (LREE/HREE = 7.27−21.07) and obvious fractionation of rare earth elements ($(La/Yb)_N$ = 8.39−38.97) implies garnet residue in source, representing higher pressure condition (Litvinovsky et al., 2000; Rapp et al., 1991). In addition, Xiong (2006) proposed that the melt coexisting with rutile has evident Nb-Ta negative anomaly under high pressure condition (depths of 50−80 km), supporting rutile residue in source where the Alaer pluton originated. In Q-Ab-Or diagram (Fig. 5f), samples fall mostly in field of 1.0−1.5 Gpa (corresponding to depths of 30−50 km). According to the crustal thickness of Altay region with an average of 56 km (Wang et al., 2004), we therefore infer that during the formation of this granite, a high-pressure magma with depths of 30−50 km was present in the middle-lower crust.

5.3. Magma source

For the possible magma source of the Triassic Alaer granite, we propose that it is likely the melting of middle-lower continental crust-derived with certain mantle input, trigged by the underplating of mantle magma. The reasons are: (1) Formation of a high-temperature granite like the Alaer granite would need hot mantle-derived magma; (2) Trace element geochemistry of the Alaer granite, such as enrichment in LREE, LILE (Rb, K) and depletion in HFSE (Nb, Ta, Ti), involvs in the melting of continental crust (Green, 1995; Barth et al., 2000); (3) The measured high Sr/Y and $(La/Yb)_N$ ratios likely record partial melting of the mafic lower crust during basaltic underplating or intrusion; (4) The late-middle Proterozoic Nd model age suggests that the source rocks may have been the old continental basement (about 1.1 Ga) rather than juvenile crust; (5) An important feature of the Central Altay terrane, where the Alaer granite is located, is that a large number of plutons there have negative ε_{Nd} (−4.2 to −0.5) and high T_{DM} values (1.0−1.3 Ga) (Wang et al., 2010), distinctly different from the Southern Altay terrane in the Chinese Altay (Fig. 6a). This illustrates that there is a relatively homogenous old continental basement for the granite formation (Wang et al., 2010); (6) I_{Sr} values of 0.706−0.709 for the Alaer granite are slightly higher than that of the average modern oceanic basalt (0.7052, Hugh, 1994). The Alaer pluton with slightly negative ε_{Nd} values is significantly different from many granites with high positive ε_{Nd} values in the CAOB (Hong et al., 2004; Jahn et al., 2000a,b), but similar to the granites located in Precambrian

https://doi.org/10.1016/j.heliyon.2019.e01261

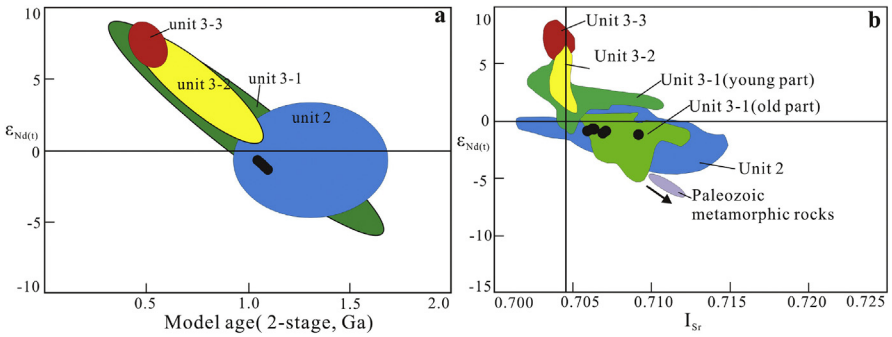

Fig. 6. $\varepsilon_{Nd(t)}$ vs. T_{DM} diagram (a) and $\varepsilon_{Nd(t)}$ vs. I_{Sr} ($(^{87}Sr/^{86}Sr)_t$) diagram (b) for the Alaer granite. The coloured areas represent the granitoids and Paleozoic metamorphic rocks from the Chinese Altay (Wang et al., 2009, 2014). T_{DM} is Nd model age. Unit 2, 3-1, 3-2 and 3-3 correspond to those of Fig. 1a. These two figures illustrate the Alaer granite could have been produced by melting of sources which were formed ca. 1.6−1.0 Ga ago and an initial melt was generated by partial melting of older continental basement or mixed with mantle-derived magma.

basement or micro-continent in the CAOB (e.g., Jahn et al., 2004; Kovalenko et al., 2004) (Fig. 6b), implying that the magma source may have been mainly originated from continental crust with certain mantle input.

The feature of the Alaer granite with low degree of differentiation suggests that its composition may represent that of parental magma and reflect the features of magma source. Experimental studies by Rapp and Watson (1995) indicated that low-degree (5−10%) dehydration melting of gabbroic rocks can produce the high Si and low-medium Al_2O_3 melts, while high-degree (20−40%) partial melting can produce felsic-intermediate melts with high Al_2O_3 content. From the relatively low SiO_2 contents (64.27−68.74 wt.%) and high Al_2O_3 contents (13.46−16.56 %) of the Alaer granite, it is suggested that the granite may have formed by high-degree (20−40%) partial melting of gabbroic rocks in old basement. This conclusion is also supported by the relatively low Fe* values (0.75−0.78, Fe* = $FeO_T/(FeO_T + MgO)$, Frost et al., 2001) of the Alaer granite because the low degree melting of gabbroic rocks can produce Fe-rich melt with high Fe* (Frost et al., 2001; Frost and Frost, 2011).

To evaluate the proportion of the juvenile component in the magma source of the Alaer granite, we postulate a melting of two end-member sources (i.e., mantle-derived basaltic rocks and old continental crust) in variable proportions. The mixing proportions for all samples can be calculated using a simple mixing equation: $X^m = Nd_c \times (\varepsilon^c - \varepsilon^s)/[\varepsilon^s \times (Nd_m - Nd_c) - (\varepsilon^m \times Nd_m - \varepsilon^c \times Nd_c)] \times 100$, where X^m represents the percentage of mantle-derived juvenile component; ε^c, ε^s and ε^m represent the Nd-isotope compositions of the crust, sample measured and mantle component, respectively. Nd_c and Nd_m represent the Nd concentrations in the crust and mantle components, respectively (Jahn et al., 2004).

https://doi.org/10.1016/j.heliyon.2019.e01261

A depleted mantle-derived basaltic rock is assumed to have ε_{Nd} (400 Ma) = +8, Nd = 15 ppm (e.g., Jahn et al., 2000a,b). The middle Paleozoic Kuerti ophiolite in the southeastern Altay contains very similar isotopic characteristics to the depleted mantle-derived basalt (Xu et al., 2003), strongly supporting the above assumption. The parameters used for the crustal component are taken from the values of ε_{Nd} (400 Ma) = −5 and Nd = 25 ppm for the widespread metamorphic rocks in the Chinese Altay (Chen and Jahn, 2002). The calculation indicates that the mantle-derived juvenile proportions were ca. 40% for the Alaer granite, consistent with the estimation by Wang et al. (2010) for the juvenile proportions of the Mesozoic anorogenic granites in the Chinese Altay. It implies that apart from the main contribution from the crustal component, there may have been substantial mantle-derived component in the formation of the Alaer granite.

5.4. Geodynamic setting

The research for the Chinese Altay tectonic evolution has been conducted by lots of scholars at home and abroad (eg., He et al., 1994; Han et al., 2004; Windley et al., 2002, 2007; Li et al., 2003; Wang et al., 2005, 2010; Li and Poliyangsiji, 2001). Their main agreement proposed that the main orogeny ended and post-collision began in the early-Permian, while new intraplate magmatism and continental breakup followed from Mesozoic, indicating the extensional setting resulted from lithosphere delamination and the underplating of great scale mantle-derived magma. In the tectonic discrimination diagram of Pearce et al. (1984), the Alaer granite plot in the within-plate granite field (Fig. 7a, b), and following synchronous large pegmatite veins with intergrowth display clearly an extensional tectonic setting.

If crust partly melts under high temperature, it implies apparently that there exists thermal anomaly at depth, and mostly under extension. The extensional case can

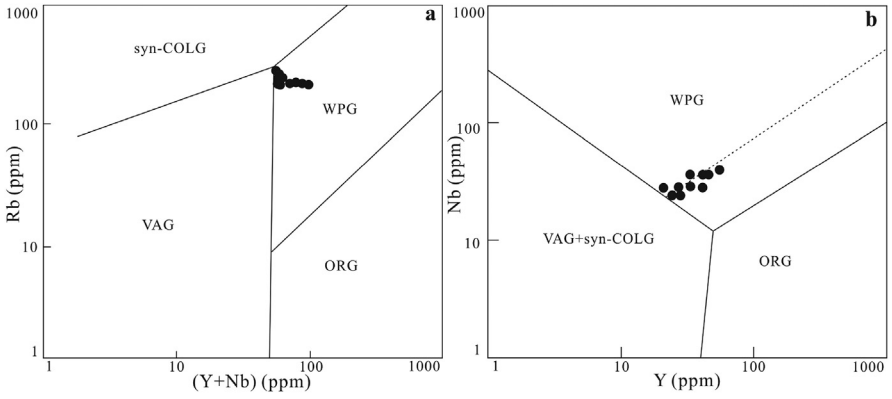

Fig. 7. Tectonic discrimination diagrams of (a) Rb vs. (Y + Nb) and (b) Nb vs. Y (after Pearce et al. (1984)). ORG- ocean ridge granite; VAG- volcanic arc granite; syn-COLG- syn-collision granite; WPG- within-plate granite.

https://doi.org/10.1016/j.heliyon.2019.e01261

appear in island arc belt under subduction and also in the upwelling of mantle plume (Wu et al., 2007). The Triassic Alaer granite is roughly synchronous with the activity of mantle-derived magma related to Siberian mantle plume (peak at 250 Ma, Franco et al., 2009; Wang et al., 2010). Does it imply that the Alaer granite resulted from the final evolution stage (Potseluev et al., 2006) or a far-field effect of this plume (Wang et al., 2014)? The Fig. 8 shows that the Alaer granite formation originated from the melting of the middle-lower crust in the Chinese Altay region, triggered by a far-field effect of Siberian mantle plume. Certainly, further works need to be done.

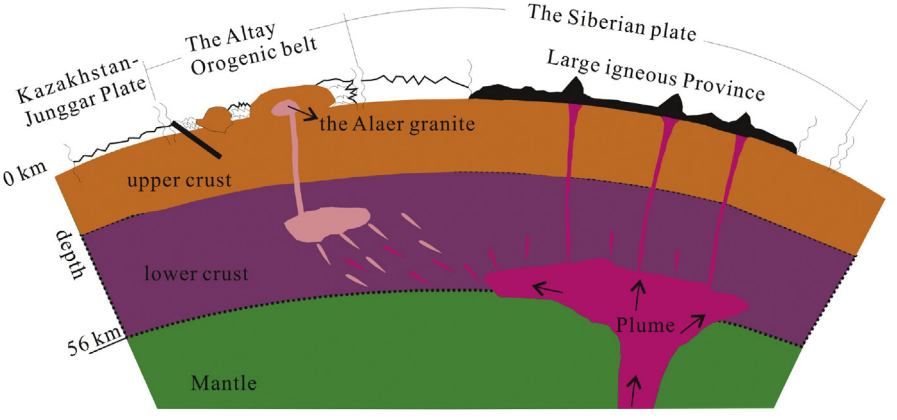

Fig. 8. Cartoon showing the formation of the Alaer granite. Underplating of mafic magma heated the base of the lower crust, generating the granitic magmas. Both crustal rocks and mantle-derived component contributed to the magma. It could result from the final evolution stage or a far-field effect of Siberian mantle plume.

6. Conclusions

(1) Intensive Triassic granitic magmatism may have occurred in the Chinese Altay.

(2) The Triassic Alaer granite belongs to I-type granite with low-degree fractionation.

(3) The Triassic Alaer granite was likely formed in an intraplate extensional setting under high temperature and pressure (829−885 °C and depths of 30−50 km), and may have originate mainly from crustal source with mantle input (caused by underplating of mantle-derived magmas).

Declarations

Author contribution statement

Feng Liu: Conceived and designed the experiments; Analyzed and interpreted the data; Wrote the paper.

Dan Han: Performed the experiments.

https://doi.org/10.1016/j.heliyon.2019.e01261

Funding statement

This study was supported by the National Key R&D Program of China (Grant No. 2017YFC0601201) and the NSFC grant (41273017).

Competing interest statement

The authors declare no conflict of interest.

Additional information

No additional information is available for this paper.

Acknowledgements

We are grateful to Suohan Tang (Institute of Geology) and the staffs (National Research Center) from Chinese Academy of Geological Sciences for their isotope and geochemistry laboratory assistance. Special thanks are given to Jianhua Liu and Jufeng Sun (Keketuohai Rare-Metal Co. Ltd) for their generous field support. Constructive reviews and suggestions by the editors and reviewers have significantly enhanced the manuscript. Cenozoic Geoscience Editing & Consultancy (Australia) is acknowledged for its scientific and language editing service.

References

Annikova, I., Vladimirov, A., Vystavnoi, S., Zhuravlev, D., Kruk, N., Lepekhina, E., Matukov, D., Moroz, E., Palesskii, S., Ponomarchuk, V., Rudnev, S., Sergeev, S., 2006. U-Pb and $^{39}Ar/^{40}Ar$ dating and Sm-Nd and Pb-Pb isotopic study of the Kalguty molybdenum-tungsten ore-magmatic system (Southern Altai). Petrology 14, 81−97.

Arth, J.G., 1976. Behaviour of trace elements during magmatic processes: a summary of theoretical models and their applications. J. Res. U. S. Geol. Surv. 4, 41−47.

Bacon, C.R., Druitt, T.H., 1988. Compositional evolution of the zoned calcalkaline magma chamber of Mount Mazama, Crater Lake, Oregon. Contrib. Mineral. Petrol. 98, 224−256.

Barth, M.G., McDonough, W.F., Rudnick, R.L., 2000. Tracking the budget of Nb and Ta in the continental crust. Chem. Geol. 165, 197−213.

Chappell, B.W., White, A.J.R., 1992. I- and S-type granites in the Lachlan Fold Belt. Trans. R. Soc. Edinb. Earth Sci. 83, 1−26.

https://doi.org/10.1016/j.heliyon.2019.e01261

Chappell, B.W., 1999. Aluminium saturation in I- and S-type granites and the characterization of fractionated haplogranites. Lithos 46, 535–551.

Chen, B., Jahn, B.M., 2002. Geochemical and isotopic studies of the sedimentary and granitic rocks of the Altai Orogen of Northwest China and their tectonic implications. Geol. Mag. 139, 1–13.

Collins, W.J., Beams, S.D., White, A.J.R., et al., 1982. Nature and origin of A-type granites with particular reference to Southeastern Australia. Contrib. Mineral. Petrol. 80, 189–200.

Coleman, R.G., 1989. Continental growth of Northwest China. Tectonics 8, 621–635.

Clemens, J.D., Stevens, G., Farina, F., 2011. The enigmatic sources of I-type granites: the peritectic connexion. Lithos 126, 174–181.

Clemens, J.D., Stevens, G., 2012. What controls chemical variation in granitic magmas? Lithos 134–135, 317–329.

Demin, A.N., Demin, P.A., Andreev, V.V., 2001. Early Mesozoic ore-bearing granitoids and their tectonic setting in the Mongolian Altay, post-collisional evolution of mobile belts. Irkutsk. In: Abstracts, International Conf. (VIIA.N. Zavaritsky Memorial Workshop). Izd. Irkutsk Univ (in Russian).

Franco, P., Richard, E.E., Alexander, S.B., Geliy, F., Evgeniy, A.N., 2009. Intraplate magmatism in Central Asia and China and associated metallogeny. Ore Geol. Rev. 35, 114–136.

Frost, B.R., Barnes, C.G., Collins, W.J., Arculus, R.J., Ellis, D.J., Frost, C.D., 2001. A geochemical classification for granitic rocks. J. Petrol. 42, 2033–2048.

Frost, C.D., Frost, B.R., 2011. On Ferroan (A-type) granitoids: their compositional variability and modes of origin. J. Petrol. 52, 39–53.

Green, T.H., 1995. Significance of Nb/Ta as an indicator of geochemical processes in the crust-mantle system. Chem. Geol. 120, 347–359.

Han, B.F., Ji, J.Q., Song, B., et al., 2004. SHRIMP zircon U-Pb ages of Kalatongke N0. 1 and Huangshandong Cu-Ni bearing mafic ultramafic complexes, North Xinjiang and geological implications. Chin. Sci. Bull. 49, 2324–2328 (in Chinese).

Han, B.F., 2008. A preliminary comparison of Mesozoic granitoids and rare metal deposits in Chinese and Russian Mountains. Acta Petrol. Sin. 24 (4), 655–660 (in Chinese with English abstract).

 https://doi.org/10.1016/j.heliyon.2019.e01261

He, G.Q., Han, B.F., Yue, Y.J., 1990. The Tectonics and Crustal Evolution of the Altay Orogen in China, 2. Geological Publishing House, Beijing, pp. 9–20. The Geological Science of Xinjiang (in Chinese).

He, G.Q., Li, M.S., Liu, D.Q., Tang, Y.L., Zhou, R.H., 1994. Paleozoic Crustal Evolution and Mineralization in Xinjiang of China. Xinjiang People's Publishing House and Educational and Cultural Press, Urumuqi and Hongkong, pp. 1–437 (in Chinese).

He, G.Q., Cheng, S.D., Xu, X., Li, J.Y., Hao, J., 2004. An Introduction to the Explanatory Text of the Map of Tectonics of Xinjiang and its Neighbouring Areas. Geological Publishing House, Beijing, pp. 1–65 (in Chinese with English abstract).

Hong, D.W., Zhang, J.S., Wang, T., et al., 2004. Continental crustal growth and the supercontinental cycle: evidence from the Central Asian Orogenic Belt. J. Asian Earth Sci. 23, 799–813.

Hugh, R.R., 1994. Using Geochemical Data: Evaluation, Presentation, Interpretation. Pearson Education Limited.

Jahn, B.M., Wu, F.Y., Chen, B., 2000a. Masssive granitoid generation in Central Asia: Nd isotopic evidence and implication for continental growth in the Phanerozoic. Episodes 23, 82–92.

Jahn, B.M., Wu, F.Y., Hong, D.W., 2000b. Important crustal growth in the Phanerozoic: isotopic evidence of granitoids from east Central Asia. Proc. Indian Acad. Sci. 109, 5–20.

Jahn, B.M., Capdevilaa, R., Liub, D., Vernona, A., Badarch, G., 2004. Sources of Phanerozoic granitoids in the Transect Bayanhongor-Ulaan Baatar, Mongolia: geochemical and Nd isotopic evidence, and implications for Phanerozoic crustal growth. J. Asian Earth Sci. 23, 629–653.

Johannes, W., Holtz, F., 1996. Petrogenesis and Experimental Petrology of Granitic Rocks. Springer, Berlin, pp. 1–335.

King, P.L., White, A.J.R., Chappell, B.W., et al., 1997. Characterization and origin of aluminous A-type granites from the Lachlan Fold Belt, Southeastern Australia. J. Petrol. 38, 371–391.

Kovalenko, V.I., Yarmolyuk, V.V., Kovach, V.P., et al., 2004. Isotope provinces, mechanisms of generation and sources of the continental crust in the Central Asian Mobile Belt: geological and isotopic evidence. J. Asian Earth Sci. 23, 605–627.

Kozlov, M.S., Khalilov, V.A., Stasenko, N.V., et al., 1991. Jurassic leucogranite-granite formation of Altai. Geol. Geofiz. 32, 44–53 (in Russian with English abstract).

https://doi.org/10.1016/j.heliyon.2019.e01261

Li, J.Y., Xiao, W.J., Wang, K.Z., Sun, G.H., Gao, L.M., 2003. Neoproterozoic-Paleozoic tectonostratigraphy, magmatic activities and tectonic evolution of eastern Xinjiang, NW China. In: Mao, J.W., Goldfarb, Seltman, Wang, X. (Eds.), Hart, Tectonic Evolution and Metallogeny of the Chinese Altay and Tianshan. IAGOD Guidebook Series 10. CERCAM/NHM, London, pp. 31−74.

Li, T.D., Poliyangsiji, B.H., 2001. Tectonics and crustal evolution of Altay in China and Kazakhstan. Xinjiang Geol. 19 (1), 27−32 (in Chinese with English abstract).

Litvinovsky, B.A., Steel, I.M., Wickham, S.M., 2000. Silicic magma formation in over-thickened crust: melting of charnockite and leucogranite at 15, 20 and 25 kbar. J. Petrol. 41, 717−737.

Liu, F., Li, Y.H., Mao, J.W., Yang, F.Q., Chai, F.M., Geng, X.X., Yang, Z.X., 2008. The SHRIMP U-Pb ages of Abagong granites in the Altai Orogen and its geological implication. Acta Geosci. Sin. 29 (6), 795−804 (in Chinese with English abstract).

Liu, F., Yang, F.Q., Mao, J.W., Chai, F.M., Geng, X.X., 2009. Study on chronology and geochemistry for Abagong granite in Altay orogeny. Acta Petrol. Sin. 25 (6), 1416−1425 (in Chinese with English abstract).

Liu, F., Zhang, Z.X., Li, Q., Qu, W.J., Li, C., 2012. New age constraints of Keketuohai pegmatite No.3 vein, Altay mountains, Northwest China: from the evidence of Re-Os and U-Pb dating. Miner. Deposits 31 (5), 1111−1118 (in Chinese with English abstract).

Liu, F., Zhang, Z.X., Li, Q., Zhang, C., Li, C., 2014a. New precise timing constraint for the Keketuohai No. 3 pegmatite in Xinjiang, China, and identification of its parental pluton. Ore Geol. Rev. 56, 209−219.

Liu, F., Cao, F., Zhang, Z.X., Li, Q., 2014b. Study on chronology and geochemistry of the granite near the Keketuohai No. 3 pegmatite in Xinjiang. Acta Petrol. Sin. 30 (1), 1−15 (in Chinese with English abstract).

Mahood, G., Hildreth, W., 1983. Large partition coefficients for trace elements in high silica rhyolites. Geochim. Cosmochim. Acta 47, 11−30.

Maniar, P.D., Piccoli, P.M., 1989. Tectonic discrimination of granitoids. Geol. Soc. Am. Bull. 101, 635−643.

Miller, C.F., Mcdowel, S.M., Mapes, R.W., 2003. Hot and cold granites? Implications of zircon saturation temperatures and preservation of inheritance. Geology 31, 529−532.

https://doi.org/10.1016/j.heliyon.2019.e01261

Mossakovsky, A.A., Ruzhentsev, S.V., Samygin, S.G., Kheraskova, T.N., 1993. The Central Asian Fold Belt: geodynamic evolution and formation history. Geotectonics 26, 455–473.

Nash, W.P., Crecraft, H.R., 1985. Partition coefficients for trace elements in silicic magmas. Geochim. Cosmochim. Acta 49, 2309–2322.

Pavlova, G.G., Borisenko, A.S., Goverdovskii, V.A., et al., 2008. Permian-Triassic magmatism and Ag-Sb mineralization in southeastern Altai and northwestern Mongolia. Russ. Geol. Geophys. 49, 545–555.

Pearce, J.A., Harris, N.B.W., Tindlem, A.G., 1984. Trace element discrimination diagrams for the tectonic interpretation of granitic rocks. J. Petrol. 25, 956–983.

Potseluev, A.A., Babkin, D.I., Kotegov, V.I., 2006. The Kalguty complex deposit, the Gorny Altai: mineralogical and geochemical characteristics and fluid regime of ore formation. Geol. Rudn. Mestorozhdenii 48, 439–459 (in Russian).

Rapp, R.P., Watson, E.B., Miller, C.F., 1991. Partial melting of amphibolite/eclogite and the origin of Archean trondhjemites and tonalities. Precambrian Res. 51, 1–25.

Rapp, R.P., Watson, E.B., 1995. Dehydration melting of metabasalt at 8–32 kbar: implications for continental growth and crust-mantle recycling. J. Petrol. 36, 891–931.

Rickwood, P.C., 1989. Boundary lines within petrologic diagrams which use oxides of major and minor elements. Lithos 22, 247–263.

Romer, R.L., Förster, H., Hahne, K., 2012. Strontium isotopes-A persistent tracer for the recycling of Gondwana crust in the Variscan Orogen. Gondwana Res. 22, 262–278.

Sengor, A.M.C., Natal'in, B.A., Burtman, V.S., 1993. Evolution of the Altaid tectonic collage and Paleozoic crustal growth in Asia. Nature 364, 299–307.

Song, P., Tong, Y., Wang, T., Qin, Q., Zhang, J.J., Ning, D.X., 2017. Zircon U-Pb ages and genetic evolution of Devonian granitic rocks in the Southeastern Chinese Altai and its tectonic implications: new evidence for magmatic evolution of calc-alkaline-high K calc-alkaline-Alkaline rocks. Acta Geol. Sin. 91 (01), 55–79 (in Chinese with English abstract).

Sun, S.S., McDonough, W.F., 1989. Chemical and isotopic systematics of oceanic basalts: implications for mantle composition and processes. Geol. Soc. Special Publ. 42, 313–345.

https://doi.org/10.1016/j.heliyon.2019.e01261

Vladimirov, A.G., Kruk, N.N., Polyanskii, O.P., et al., 2005. Correlation of Hercynian deformations, sedimentation and magmatism in the Altai collisional system as reflecting plate- and plum- tectonics. Prob. Tect. Cent. Asia Moscow Geos 1277–1308 (in Russian).

Wang, Y.X., Han, G.H., Jiang, M., Yuan, X.C., Walter, D.M., Robert, G.C., 2004. Crustal structure along the geosciences transect from Altay to AltunTagh. Chin. J. Geophys. 47 (2), 240–249 (in Chinese with English abstract).

Wang, T., Hong, D.W., Tong, Y., Han, B.F., Shi, Y.R., 2005. Zircon U-Pb SHRIMP age and origin of post-orogenic Lamazhao granitic pluton from Altai Orogen: its implications for vertical continental growth. Acta Petrol. Sin. 21 (3), 640–650 (in Chinese with English abstract).

Wang, T., Hong, D.W., Jahn, B.M., Tong, Y., Wang, Y.B., Han, B.F., Wang, X.X., 2006. Timing, petrogenesis, and setting of Paleozoic synorogenic intrusions from the Altai mountains, Northwest China: implications for the tectonic evolution of an accretionary orogeny. J. Geol. 114, 735–751.

Wang, T., Jahn, B.M., Kovach, V.P., et al., 2008. Mesozoic anorogenic granitic magmatism in the Altai Paleozoic accretionary orogen, NW China, and its implications for crustal architecture and growth. In: Abstract SE53-A010, AOGS 5th Annual General Meeting. Busan, Korea.

Wang, T., Jahn, B.M., Victor, P.K., Tong, Y., Hong, D.W., Han, B.F., 2009. Nd-Sr isotopic mapping of the Chinese Altai and implications for continental growth in the Central Asian Orogenic Belt. Lithos 110, 359–372.

Wang, T., Tong, Y., Li, S., Zhang, J.J., Shi, X.J., Li, J.Y., Han, B.F., Hong, D.W., 2010. Spatial and temporal variations of granitoids in the Altay Orogen and their implications for tectonic setting and crustal growth: perspectives from Chinese Altay. Acta Petrol. Mineral. 29 (6), 595–618 (in Chinese with English abstract).

Wang, T., Jahn, B.M., Victor, P.K., Tong, Y., Simon, A.W., Hong, D.W., Li, S., Ekaterina, B.S., 2014. Mesozoic intraplate granitic magmatism in the Altai accretionary orogeny, NW China: implications for the orogenic architecture and crustal growth. Am. J. Sci. 314, 1–42.

Watson, E.B., Harrison, T.M., 1983. Zircon saturation revisited: temperature and composition effects in a variety of crustal magma types. Earth Planet. Sci. Lett. 64, 295–304.

Whalen, J.B., Currie, K.L., Chappell, B.W., 1987. A-type granites: geochemical characteristics discrimination and petrogenesis. Contrib. Mineral. Petrol. 95, 407–419.

https://doi.org/10.1016/j.heliyon.2019.e01261

Weaver, B.L., Tarney, J., 1984. Empirical approach to estimating the composition of the continental crust. Nature 310, 575–577.

Windley, B.F., Kroener, A., Guo, J., Qu, G., Li, Y., Zhang, C., 2002. Neoproterozoic to Paleozoic geology of the Altai Orogen, NW China: new zircon age data and tectonic evolution. J. Geol. 110, 719–737.

Windley, B.F., Alexeiev, D., Xiao, Wenjiao, Kröner, A., Badarch, G., 2007. Tectonic models for accretion of the Central Asian Orogenic Belt. J. Geol. Soc. 164, 31–47.

Wu, F.Y., Li, X.H., Yang, J.H., Zheng, Y.F., 2007. Discussions on the petrogenesis of granites. Acta Petrol. Sin. 23 (6), 1217–1238 (in Chinese with English abstract).

Xiao, W.J., Huang, B.C., Han, C.M., Sun, S., Li, J.L., 2010. A review of the western part of the Altaids: a key to understanding the architecture of accretionary orogens. Gondwana Res. 18, 253–273.

Xiong, X.L., 2006. Trace element evidence for growth of early continental crust by melting of rutile-bearing hydrous eclogite. Geology 34, 945–948.

Xu, J.F., Castillo, P.R., Chen, F.R., Niu, H.C., Yu, X.Y., Zhen, Z.P., 2003. Geochemistry of late Palaeozoic mafic igneous rocks from the Kuerti area, Xinjiang, Northwest China: implications for back-arc mantle evolution. Chem. Geol. 193, 137–154.

Yang, J.H., Sun, J.F., Zhang, M., Wu, F.Y., Wilde, S.A., 2012. Petrogenesis of silica-saturated and silica-undersaturated syenites in the northern North China Craton related to post-collisional and intraplate extension. Chem. Geol. 328, 149–167.

Zhou, T.X., Chen, J.F., Xie, Z., Zhang, X., Yang, X.C., Chen, F.M., 2000. Isotopic geochemistry of granitic rocks from Tuomuer peak region, Tianshan, China. Acta Petrol. Sin. 16 (2), 153–160 (in Chinese with English abstract).

Zhu, Y.F., Zeng, Y.S., Gu, L.B., 2006. Geochemistry of the rare metal-bearing pegmatite No. 3 vein and related granites in the Keketuohai region, Altay mountains, Northwest China. J. Asian Earth Sci. 27, 61–77.

Zhu, Y.F., 2007. Indosinian movement and metallogeny in Xinjiang, China. Geol. Bull. China 26, 510–519 (in Chinese with English abstract).

Zou, T.R., Li, Q.C., 2006. The Rare Metal and the REE Deposits in Xinjiang. Geological Publishing House, Beijing, China, pp. 34–51 (in Chinese).

https://doi.org/10.1016/j.heliyon.2019.e01261